




Cite this: *RSC Adv.*, 2018, 8, 1351

# Magnetic CoFe<sub>2</sub>O<sub>4</sub> nanoparticles supported on graphene oxide (CoFe<sub>2</sub>O<sub>4</sub>/GO) with high catalytic activity for peroxymonosulfate activation and degradation of rhodamine B

Rida Tabit,<sup>a</sup> Othmane Amadine,<sup>b</sup> Younes Essamlali,<sup>b</sup> Karim Dânoune,<sup>b</sup> Abdallah Rhihil<sup>a</sup> and Mohamed Zahouily \*<sup>ab</sup>

Herein, we report the preparation of magnetic CoFe<sub>2</sub>O<sub>4</sub> nanoparticles and CoFe<sub>2</sub>O<sub>4</sub>/graphene oxide (GO) hybrids and evaluate their catalytic activity as heterogeneous peroxymonosulfate (PMS) activators for the decomposition of rhodamine B. The surface morphologies and structures of both CoFe<sub>2</sub>O<sub>4</sub> nanoparticles and CoFe<sub>2</sub>O<sub>4</sub>/GO hybrids were investigated by powder X-ray diffraction (XRD), scanning electron microscopy (SEM), energy-dispersive X-ray spectroscopy (EDS), Fourier transform infrared spectroscopy (FTIR) and nitrogen adsorption–desorption isotherms. The magnetic properties of the samples were assessed using a SQUID magnetometer at 298 K. Catalytic oxidation experiments demonstrated that CoFe<sub>2</sub>O<sub>4</sub>/GO hybrids exhibited much better catalytic activity than CoFe<sub>2</sub>O<sub>4</sub> nanoparticles or CoFe<sub>2</sub>O<sub>4</sub>/reduced graphene oxide (rGO) hybrids, suggesting that GO plays an important role in CoFe<sub>2</sub>O<sub>4</sub>/GO hybrids in the decomposition of rhodamine B. The influence of various reaction conditions such as temperature, concentration of PMS, pH and decomposition time of rhodamine B over the CoFe<sub>2</sub>O<sub>4</sub>/GO catalyst were investigated and optimized. The rhodamine B degradation process was found to fit a pseudo-first order kinetics model. The catalyst could be easily separated from the reaction mixture by applying an external magnet. In particular, the as-prepared CoFe<sub>2</sub>O<sub>4</sub>/GO hybrid exhibited good reusability and stability in successive degradation experiments in PMS solution.

Received 6th September 2017  
 Accepted 15th December 2017

DOI: 10.1039/c7ra09949e

rsc.li/rsc-advances

## 1. Introduction

The dye industry discharges large amounts of industrial wastewater and hence, it is one of the major sources of organic pollutants. Nowadays, there are more than 100 000 dyes belonging to various chemical classes with an annual production of 7.105 tons.<sup>1</sup> It is estimated that 10–15% of initial quantities are lost during dyeing procedures, which are discharged without prior treatment to the effluent; this contaminates groundwater and is toxic to humans and animals. Most of these compounds are chemically stable and have a complicated constitution, which makes them resistant to photo- and biological degradation. The Rhodamine (RhB) dye is one of fresh peach of synthetic dyes that is widely used as a colorant in the manufacturing of textiles and foodstuffs. It has been medically proven that rhodamine dye is harmful and toxic to humans and animals, and causes irritation of the skin, eyes and respiratory tract.<sup>2</sup> Due to its high toxicity and negative effects on public health, various physical, chemical and

biological approaches have been extensively explored and investigated for the removal of organic dyes from wastewater including adsorption, coagulation, biological degradation and filtration processes as well as chemical oxidation by hydro chlorite and Fenton methods.<sup>3</sup> However, these methods suffer from different drawbacks that are primarily associated with the cost-intensive production of oxidants, instability during long reaction times, short lifetime and pH adjustments.

In recent years, sulfate radical-based oxidation processes have received much attention<sup>4</sup> for its efficient degradation of organic contaminants. The sulfate radical (SO<sup>•4-</sup>) generated from peroxymonosulfate, as an alternative to the hydroxyl radical (OH<sup>•</sup>), is a strong oxidant with a high redox potential. It can react with many organic contaminants to yield a degradation performance similar to that expected for the hydroxyl radical (OH<sup>•</sup>). The activation processes of PMS can be achieved using heat, ultraviolet irradiation, transition metals, or metal oxides,<sup>5–7</sup> which are similar to the cases involving hydrogen peroxide. Recently, the Co<sup>2+</sup> ion coupled with a PMS system for the degradation of organic contaminants has attracted tremendous interest since it exhibits better efficiencies than the Fenton reaction.<sup>8,9</sup> Despite the advantages of this homogeneous activation process, the application of this method in water treatment is limited due to

<sup>a</sup>Laboratoire de Matériaux, Catalyse & Valorisation des Ressources Naturelles, URAC 24, Faculté des Sciences et Techniques, Université Hassan II, Casablanca B.P. 146, 20650, Morocco. E-mail: m.zahouily@mascir.com; Tel: +212 661416359

<sup>b</sup>MASCiR Foundation, VARENA Center, Rabat Design, Rue Mohamed El Jazouli, Madinat Al Irfane 10100 Rabat, Morocco





containing 50 mL of RhB solution at room temperature (25 °C). In a typical procedure, 0.005 g of oxone was first added to RhB solution under constant stirring. Then, 0.010 g of catalyst was added to start the reaction. At a given time interval, a pre-determined amount (2.0 mL) of solution was withdrawn into a vial fitted with a micro-filter (45 μm) for solid catalyst removal. The concentrations of RhB were determined by monitoring the decrease in absorbance at the maximum wavelength (554 nm) with UV-vis spectroscopy.

The degradation efficiency was calculated according to the following equation:

$$\text{Degradation}(\%) = \frac{(C_0 - C) \times 100}{C_0} = \frac{(A_0 - A) \times 100}{A_0}$$

where,  $C_0$  and  $C$  are the initial and final concentrations of RhB, respectively, and  $A_0$  and  $A$  represent the initial and the final absorbance of RhB at 554 nm, respectively.

### 3. Results and discussion

XRD was employed to analyze the crystalline phases of as-prepared GO,  $\text{CoFe}_2\text{O}_4$  and  $\text{CoFe}_2\text{O}_4/\text{GO}$  samples (Fig. 1). The XRD patterns (Fig. 1a) confirmed the successful oxidation of natural graphite to graphite oxide, which exhibits a strong diffraction peak at  $2\theta = 10.28$ , corresponding to the (001) inter-planar spacing of 0.87 nm, which is much larger than the  $d$ -spacing of graphite (0.34 nm). It is evident that  $\text{CoFe}_2\text{O}_4$  and  $\text{CoFe}_2\text{O}_4/\text{GO}$  exhibit similar XRD patterns. The diffraction peaks for the two samples at  $2\theta = 30.3, 35.6, 43.3, 53.6, 57.1$  and  $62.8$  are consistent with the (220), (311), (400), (422), (333) and (440) reflections, respectively, of the cubic spinel-type structure of  $\text{CoFe}_2\text{O}_4$  (JCPDS 75-0033). It should be noted that typical diffraction peaks of GO could not be detected in the XRD pattern of  $\text{CoFe}_2\text{O}_4/\text{GO}$ , suggesting the destruction of the regular layered structure of GO due to the crystal growth of  $\text{CoFe}_2\text{O}_4$  between its inter-layers. The average crystallite size of

$\text{CoFe}_2\text{O}_4$  and  $\text{CoFe}_2\text{O}_4/\text{GO}$ , estimated from the Debye–Scherrer formula, are 10.37 and 11.06 nm, respectively.

The FT-IR spectra of GO,  $\text{CoFe}_2\text{O}_4$  and  $\text{CoFe}_2\text{O}_4/\text{GO}$  are shown in Fig. 2. As illustrated in Fig. 2, several characteristic bands of the functional groups of GO can be observed. The two peaks located at 1725 and 1618  $\text{cm}^{-1}$  are assigned to the anti-symmetric and symmetric stretching vibrations of carboxylic groups ( $\text{COO}^-$ ). The absorption peaks at 1035  $\text{cm}^{-1}$  is attributed to the stretching vibrations of alkoxy C–O from the oxygen-containing functional groups such as carbonyl, carboxylic and epoxy groups.<sup>35</sup> Indeed, the FTIR spectrum of  $\text{CoFe}_2\text{O}_4$  shows a peak at 577  $\text{cm}^{-1}$ , which is ascribed to the Co–O and Fe–O vibrations. It is worth noting that in the spectrum of  $\text{CoFe}_2\text{O}_4/\text{GO}$ , the peaks at 1618  $\text{cm}^{-1}$ , corresponding to the functional groups of COO in GO, shifts to 1567  $\text{cm}^{-1}$ .

The calculated textural parameters of  $\text{CoFe}_2\text{O}_4$  and  $\text{CoFe}_2\text{O}_4/\text{GO}$  are summarized in Table 1. From the data in Table 1, it can be seen that the BET surface area of  $\text{CoFe}_2\text{O}_4$  is 124  $\text{m}^2 \text{g}^{-1}$  and its pore volume is 0.1662  $\text{cm}^3 \text{g}^{-1}$ , while the surface area of the  $\text{CoFe}_2\text{O}_4/\text{GO}$  is 142  $\text{m}^2 \text{g}^{-1}$  and its pore volume is 0.1868  $\text{cm}^3 \text{g}^{-1}$ . The addition of GO nanosheets should be the responsible for this increase in the surface area of  $\text{CoFe}_2\text{O}_4/\text{GO}$  compared to that of  $\text{CoFe}_2\text{O}_4$ . The nitrogen sorption isotherm of  $\text{CoFe}_2\text{O}_4$ , as shown in Fig. 3, is of type III with a distinct hysteresis loop of type H2 in the relative pressure range of 0.5 and extending almost to 1, which is characteristic of mesoporous textural porosity. The corresponding pore size distribution curve indicates that  $\text{CoFe}_2\text{O}_4$  exhibited a pore size distribution in the range of 2 to 10 nm with a central value of 6.5 nm, corresponding to mesoporous materials. As for  $\text{CoFe}_2\text{O}_4/\text{GO}$ , there is a slight difference as the nitrogen sorption isotherms of  $\text{CoFe}_2\text{O}_4/\text{GO}$  are of the type III (Fig. 3) and the hysteresis loop is of type H3 according to the IUPAC classification. The corresponding pore size distribution curve indicates that  $\text{CoFe}_2\text{O}_4/\text{GO}$  has a centralized pore size distribution within two areas toward 4 and 6 nm, which confirm the existence of textural mesopores.

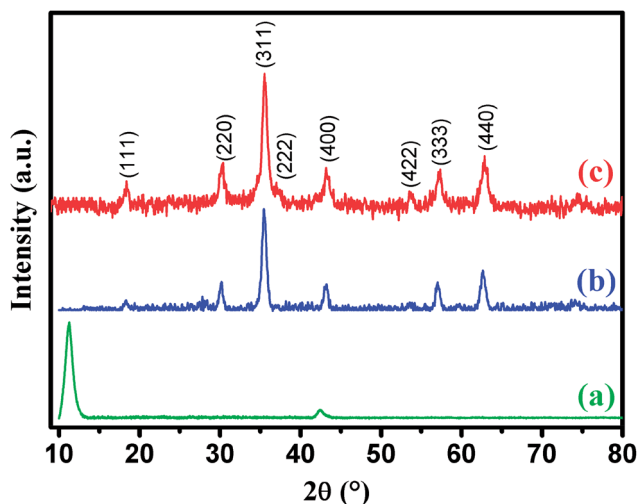


Fig. 1 XRD patterns of graphene oxide (a),  $\text{CoFe}_2\text{O}_4$  (b) and  $\text{CoFe}_2\text{O}_4/\text{GO}$  (c).



Fig. 2 FT-IR spectra of GO,  $\text{CoFe}_2\text{O}_4$  and  $\text{CoFe}_2\text{O}_4/\text{GO}$ .



Table 1 Lattice parameter, crystallite size, BET surface area and pore volume of the CoFe<sub>2</sub>O<sub>4</sub> and CoFe<sub>2</sub>O<sub>4</sub>/GO samples

Samples	Lattice parameter <i>a</i> (Å)	Cell volume (Å <sup>3</sup> )	Crystallite size <sup>a</sup> /nm	<i>S</i> <sub>BET</sub> <sup>b</sup> /m <sup>2</sup> g <sup>-1</sup>	<i>V</i> <sub>meso</sub> <sup>b</sup> /mL g <sup>-1</sup>	<i>D</i> <sub>meso</sub> <sup>b</sup> /nm
CoFe <sub>2</sub> O <sub>4</sub>	8.399	592.50	10.37	124	0.1662	6.5
CoFe <sub>2</sub> O <sub>4</sub> /GO	8.354	583.02	11.06	142	0.1868	4.6

<sup>a</sup> Calculated by the Debye–Scherer equation. <sup>b</sup> From nitrogen sorption analysis.

The surface morphology and elemental composition of the as-prepared CoFe<sub>2</sub>O<sub>4</sub> and CoFe<sub>2</sub>O<sub>4</sub>/GO were investigated by SEM and EDX. From the SEM images, as shown in Fig. 4, it could be observed that CoFe<sub>2</sub>O<sub>4</sub> exhibits a heterogeneous microstructure that consisted of crystallites of various sizes. It should be noted that particles of CoFe<sub>2</sub>O<sub>4</sub> are strongly agglomerated as shown in the FE-SEM images in (Fig. 4b), which can be attributed to the powerful inherent magnetic interaction of CoFe<sub>2</sub>O<sub>4</sub> magnetic particles. Furthermore, as shown in Fig. 4c and d, when CoFe<sub>2</sub>O<sub>4</sub> was supported on the surface of GO nanosheets, the agglomeration phenomenon reduced, suggesting that GO can prevent the aggregation of the CoFe<sub>2</sub>O<sub>4</sub> nanoparticles. Moreover, energy dispersive X-ray (EDX) analyses were recorded and are shown Fig. 4e. The EDX analysis confirmed the elemental composition of the CoFe<sub>2</sub>O<sub>4</sub>–GO material, which primarily consists of C, Co, Fe, and O. The chemical composition of the as-synthesized products was further analyzed by inductively coupled plasma atomic emission spectroscopy (ICP-AES).

Table 2 shows the elemental composition of CoFe<sub>2</sub>O<sub>4</sub>/GO measured by EDX, ICP-AES and C.A. The stoichiometric elemental composition for Co, Fe, and O is 22.79, 44.44, and 4.32%, respectively. In all samples, Co and Fe are in the ratio of 1 : 2, which further confirm the structure of CoFe<sub>2</sub>O<sub>4</sub>/GO.

The morphology of GO and CoFe<sub>2</sub>O<sub>4</sub>/GO was characterized by STEM. From Fig. 5(a and b), it can be observed that CoFe<sub>2</sub>O<sub>4</sub> NPs prepared in the absence of GO show spherical particles with severe aggregation due to the magnetic dipolar interaction among the magnetite NPs. In comparison, uniform CoFe<sub>2</sub>O<sub>4</sub> NPs are deposited and well-dispersed on the basal planes of graphene (Fig. 5(c and d)). In addition, we noticed that CoFe<sub>2</sub>O<sub>4</sub> NPs were still tightly anchored on the surface of GO even after sample preparation (mechanical stirring and sonication) for STEM analysis, suggesting a strong interaction between CoFe<sub>2</sub>O<sub>4</sub> NPs and GO. Moreover, the graphene sheets distributed between the CoFe<sub>2</sub>O<sub>4</sub> NP can prevent the aggregation of

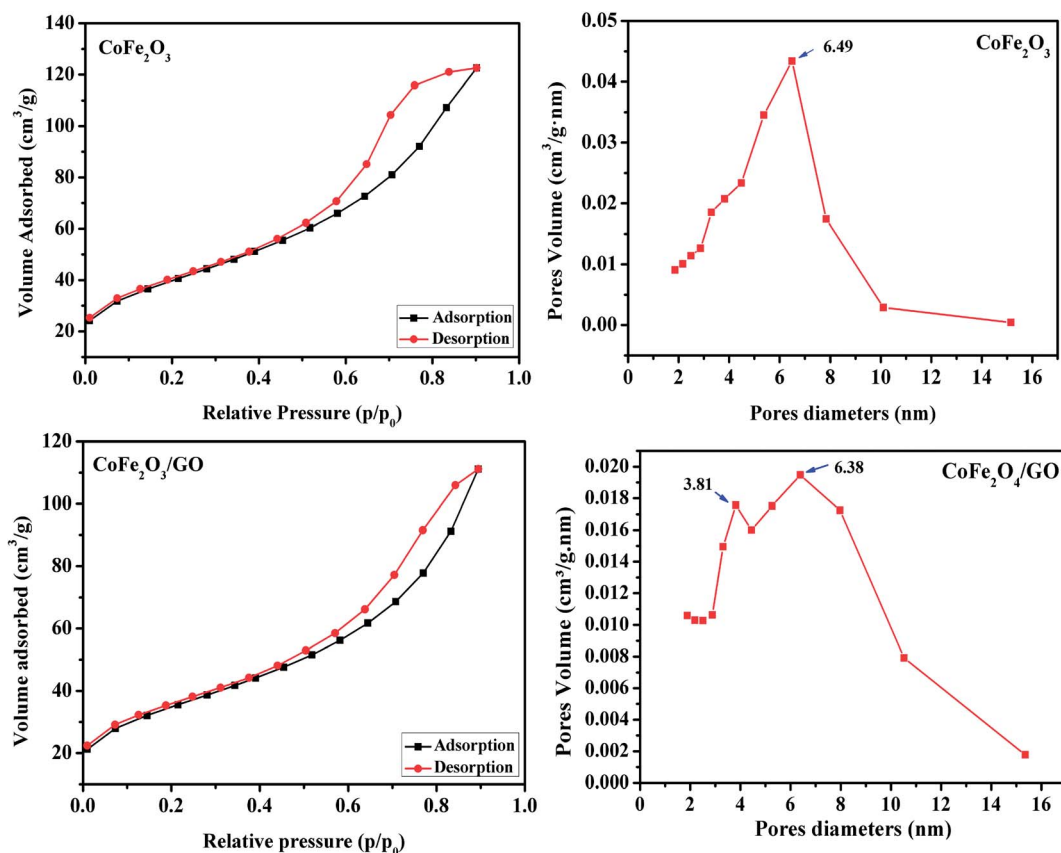


Fig. 3 Nitrogen adsorption/desorption isotherms and BJH pore size distribution of CoFe<sub>2</sub>O<sub>4</sub> and CoFe<sub>2</sub>O<sub>4</sub>/GO.



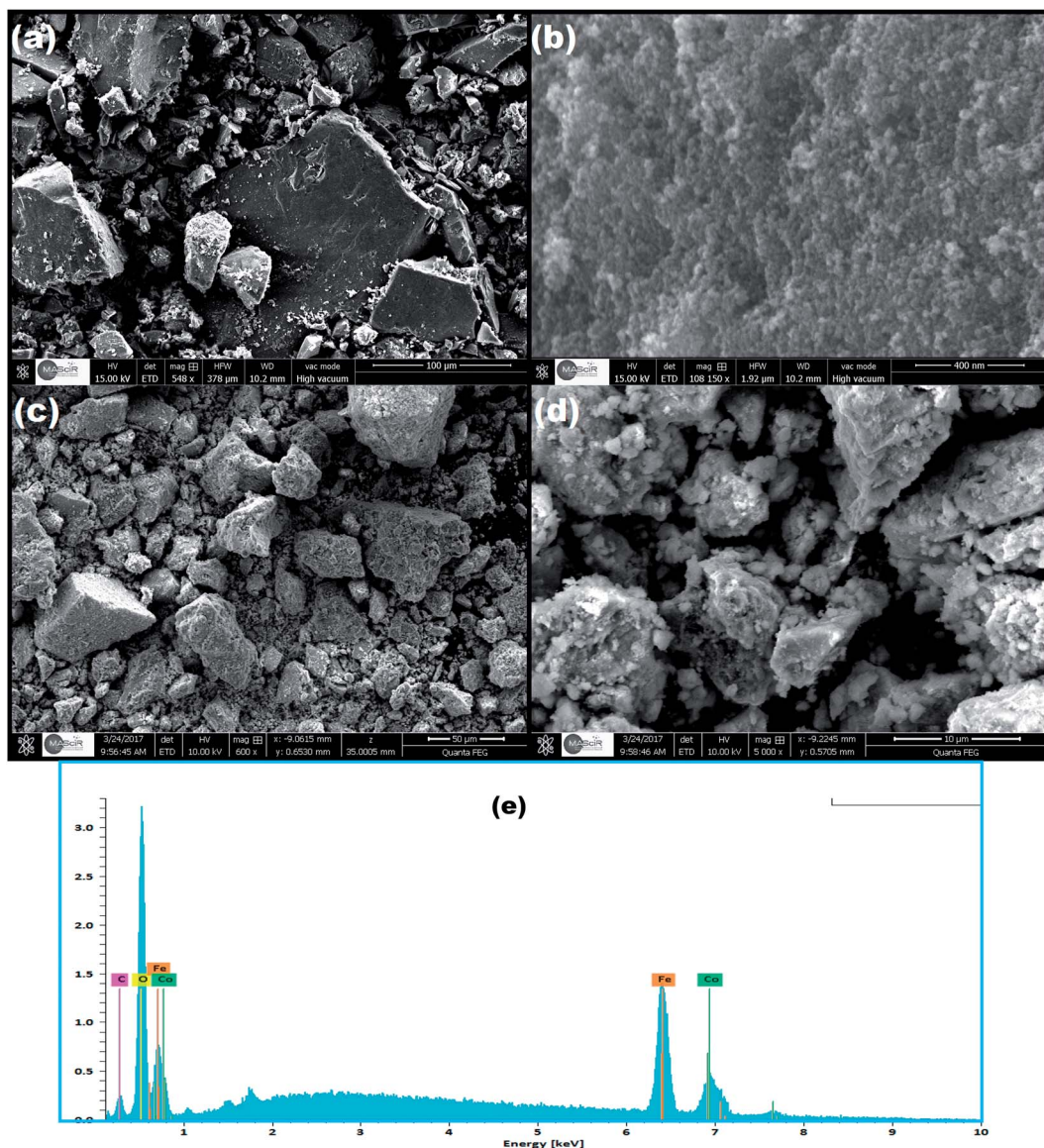


Fig. 4 SEM images of (a, b)  $\text{CoFe}_2\text{O}_4$  and (c, d)  $\text{CoFe}_2\text{O}_4/\text{GO}$ , (e) EDX of  $\text{CoFe}_2\text{O}_4/\text{GO}$ .

Table 2 Elemental composition of  $\text{CoFe}_2\text{O}_4/\text{GO}$  measured by EDX, ICP-AES and C.A

Element	Weight (%)		
	EDX	ICP-AES	C.A
Co	22.15	22.79	—
Fe	45.94	44.44	—
C	4.24	—	4.32
O	37.65	—	—

$\text{CoFe}_2\text{O}_4$  NP to a certain extent, which can be of great benefit to reactions.

The magnetic properties of  $\text{CoFe}_2\text{O}_4$  and  $\text{CoFe}_2\text{O}_4/\text{GO}$  were investigated by SQUID from  $-15\,000$  to  $15\,000$  Oe at room temperature as shown in Fig. 6. The saturation magnetization

( $M_s$ ) of  $\text{CoFe}_2\text{O}_4$  is close to  $47.33\text{ emu g}^{-1}$ , which is higher than that corresponding to the  $\text{CoFe}_2\text{O}_4/\text{GO}$  material ( $30.15\text{ emu g}^{-1}$ ). This increase in  $M_s$  value could be due to (i) the existence of the GO nanosheets, (ii) the surface defect of  $\text{CoFe}_2\text{O}_4$  crystallites and (iii) the strong interfacial interaction between  $\text{CoFe}_2\text{O}_4$  nanoparticles and GO surfaces. Moreover, the field-dependent magnetization curves of  $\text{CoFe}_2\text{O}_4$  and  $\text{CoFe}_2\text{O}_4/\text{GO}$  show non-negligible remanence ( $M_r$ ) and coercivity ( $H_c$ ), indicating paramagnetic behavior of the two samples at room temperature (Table 3). Furthermore,  $\text{CoFe}_2\text{O}_4/\text{GO}$  hybrids can be easily separated from the reaction by applying an external magnetic field. The  $\text{CoFe}_2\text{O}_4/\text{GO}$  catalyst can be dispersed in deionized water to form a stable brown homogenous suspension before magnetic separation (inset of Fig. 6a). However, when a magnet was placed close to the reaction vessel, it could be observed that the synthesized samples were rapidly attracted,



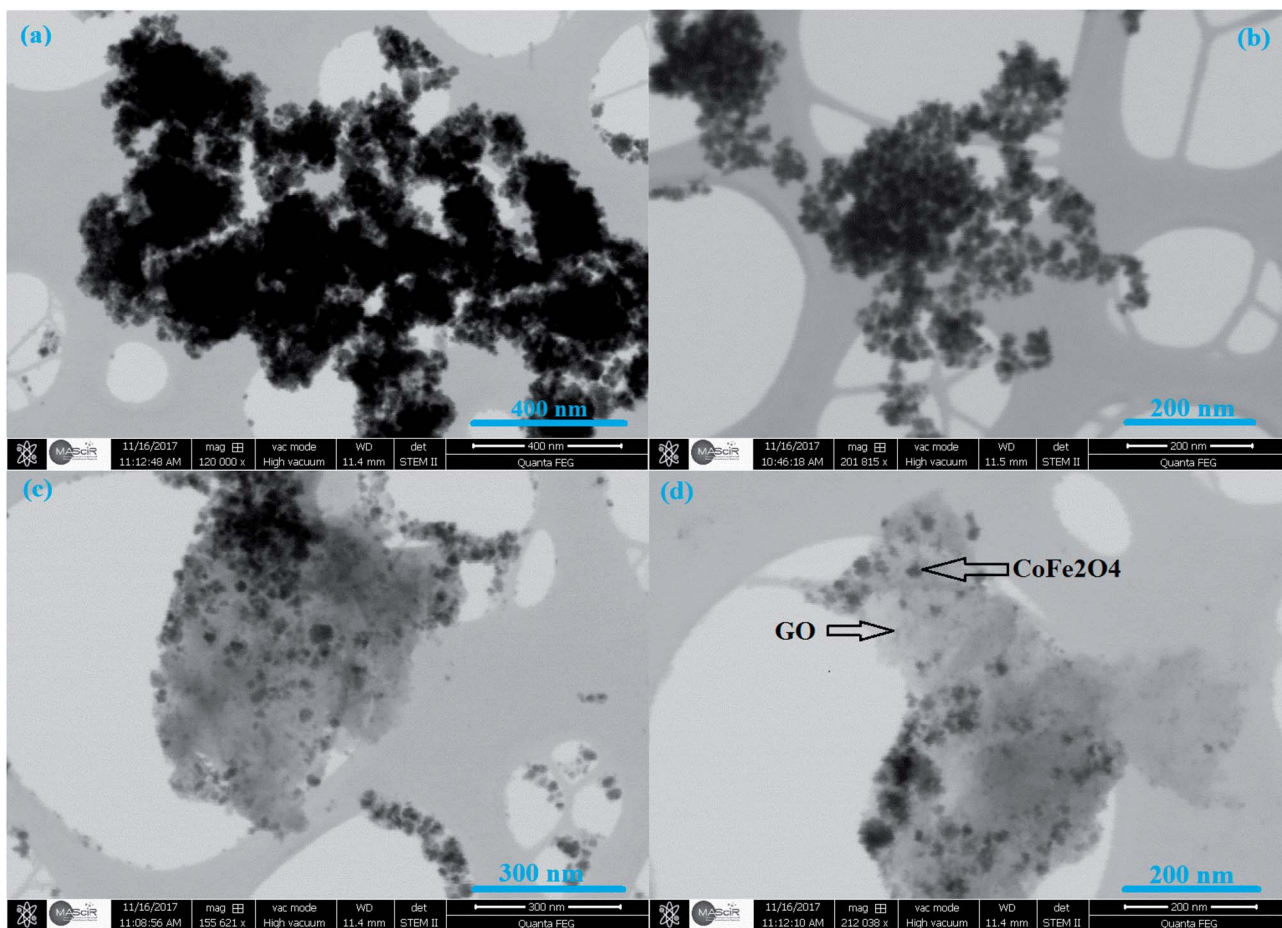


Fig. 5 STEM images of  $\text{CoFe}_2\text{O}_4$  (a, b) and  $\text{CoFe}_2\text{O}_4/\text{GO}$  (c, d).



Fig. 6 Magnetization curves of  $\text{CoFe}_2\text{O}_4$  and  $\text{CoFe}_2\text{O}_4/\text{GO}$ . The inset shows the photographs of the separation processes of  $\text{CoFe}_2\text{O}_4/\text{GO}$ : (a) without external magnetic field, and (b, c) with external magnetic field.

and a nearly colorless solution was obtained (inset of Fig. 6(b and c)).

To evaluate the catalytic performance of our materials, the degradation of RhB in the presence of the PMS was selected as

a model catalytic reaction. The degradation kinetics of RhB in aqueous solution was studied by monitoring the decrease of its absorption peak at 554 nm in the UV-vis spectra with time as exemplified in Fig. 7a. No significant shift in the absorption peak ( $\lambda_{\text{max}} = 554 \text{ nm}$ ) was observed before 12 min except for a quick reduction in the absorbance at 554 nm. Since the absorbance at 554 nm was primarily attributed to RhB remaining in the solution under our experimental conditions, the linear relationship between the concentration of the residual RhB and its absorbance at 554 nm was further verified by the standard calibration curve ( $R^2 = 0.9970$ ), and the corresponding absorbance was then converted to the RhB concentration in the solution used for kinetic analysis. To further investigate the degradation of RhB, total organic carbon (TOC), which has been widely used to evaluate the degree of

Table 3 The values of saturation magnetization ( $M_s$ ), remanent magnetization ( $M_r$ ) and coercivity ( $H_c$ ) of  $\text{CoFe}_2\text{O}_4$  and  $\text{CoFe}_2\text{O}_4/\text{GO}$ , extracted from Fig. 5

Sample	$M_s$ ( $\text{emu g}^{-1}$ )	$M_r$ ( $\text{emu g}^{-1}$ )	$H_c$ (Oe)
$\text{CoFe}_2\text{O}_4$	47.33	8.55	348.53
$\text{CoFe}_2\text{O}_4/\text{GO}$	30.15	9.78	897.16



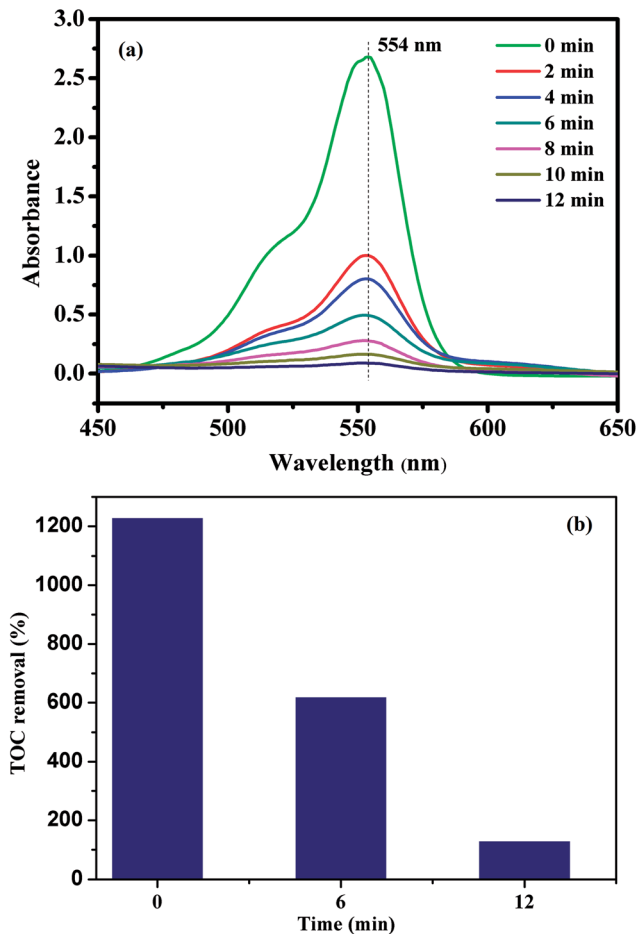


Fig. 7 UV-vis spectra of RhB solution at different times using  $\text{CoFe}_2\text{O}_4/\text{GO}$  as a catalyst (a); the TOC removal efficiency of RhB using  $\text{CoFe}_2\text{O}_4/\text{GO}$  as a catalyst.

mineralization of organic species, was measured in the RhB degradation process by the  $\text{CoFe}_2\text{O}_4/\text{GO}/\text{PMS}$  system as shown in Fig. 7b. The TOC removal efficiency of RhB reached 89.34% after 12 min in the presence of the  $\text{CoFe}_2\text{O}_4/\text{GO}/\text{PMS}$  system, which confirms that RhB could be mineralized to residual organic molecules by the as-prepared samples.

As shown in Fig. 8, no RhB degradation was observed *via* PMS oxidation alone. Similarly,  $\text{CoFe}_2\text{O}_4$ ,  $\text{CoFe}_2\text{O}_4/\text{rGO}$  and  $\text{CoFe}_2\text{O}_4/\text{GO}$  cannot catalyze RhB degradation in the absence of PMS, which reveals that the contribution from simple physical adsorption is negligible in this case. Moreover, in the absence of a catalyst, the concentration of RhB remained unchanged over time, suggesting that it is difficult for the degradation of RhB to proceed without a catalyst. Therefore, the degradation of RhB is very sensitive to the presence of both PMS and catalyst in the reaction system. The catalytic performances of  $\text{CoFe}_2\text{O}_4$ ,  $\text{CoFe}_2\text{O}_4/\text{rGO}$  and  $\text{CoFe}_2\text{O}_4/\text{GO}$  for the degradation of RhB with PMS were clearly different in the three samples and the degradation efficiencies were 78, 90 and 98%, respectively. Moreover, it can be clearly observed that the degradation rate of RhB over  $\text{CoFe}_2\text{O}_4/\text{GO}$  was much faster than that corresponding to  $\text{CoFe}_2\text{O}_4/\text{rGO}$  and  $\text{CoFe}_2\text{O}_4$  and it took around 12 min for

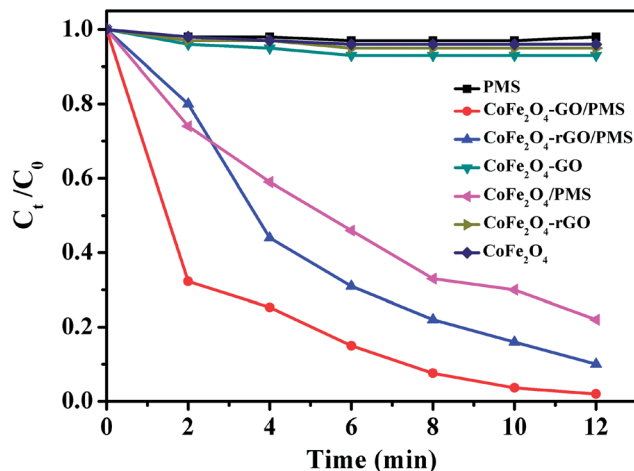


Fig. 8 RhB degradation by various catalytic PMS systems. Conditions:  $[\text{RhB}]_0 = 0.03 \text{ mmol L}^{-1}$ ,  $[\text{PMS}] = 0.10 \text{ mg L}^{-1}$ , amount of catalyst = 10 mg, temperature =  $25^\circ\text{C}$ .

complete removal of RhB. This superior catalytic activity of  $\text{CoFe}_2\text{O}_4/\text{GO}$  could be related to the electronic structure and the presence of functional hydroxyl groups in GO, which could be involved in the degradation mechanism, thus enhancing the catalytic activity of the  $\text{CoFe}_2\text{O}_4/\text{GO}$  catalyst for the degradation of RhB. As compared with  $\text{CoFe}_2\text{O}_4$ , GO can offer an environment to prevent aggregation of  $\text{CoFe}_2\text{O}_4$  nanoparticles and also a higher surface area ( $142 \text{ m}^2 \text{ g}^{-1}$ ) ( $124 \text{ m}^2 \text{ g}^{-1}$ ), which can provide more active sites for catalytic degradation of RhB.

Fig. 9 shows the linear kinetic fitting plots of  $\ln(C_0/C_t) = f(t)$  for RhB photodegradation, in which  $C_0$  and  $C_t$  are the initial concentration of RhB and its concentration at time  $t$ , respectively. In general, the degradation of organic dyes obeys a pseudo-first order kinetics model. As shown in Fig. 9, RhB degradation by  $\text{CoFe}_2\text{O}_4$ ,  $\text{CoFe}_2\text{O}_4/\text{GO}$  and  $\text{CoFe}_2\text{O}_4/\text{rGO}$  can follow a pseudo-first order kinetics model. Furthermore, the constant rate values indicate that  $\text{CoFe}_2\text{O}_4/\text{GO}$  possesses

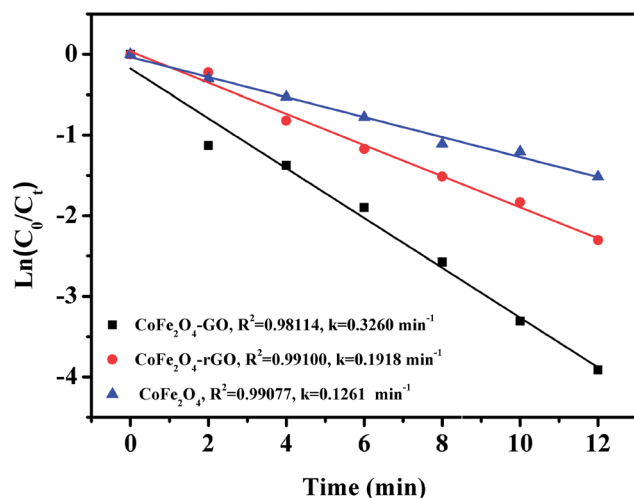


Fig. 9 Linear kinetic fitting plots of  $\ln(C_0/C_t) = f(t)$  based on a first-order kinetic model.



a better rate constant ( $0.3260 \text{ min}^{-1}$ ) than  $\text{CoFe}_2\text{O}_4/\text{rGO}$  ( $0.1918 \text{ min}^{-1}$ ) and  $\text{CoFe}_2\text{O}_4$  ( $0.1261 \text{ min}^{-1}$ ), suggesting that graphene oxide plays a significant role in the enhancement of PMS catalytic degradation of RhB. The strong interfacial interaction between graphene oxide and  $\text{CoFe}_2\text{O}_4$  generates a synergistic function of large surface area and improves the electron transport ability and chemical reaction sites.

The effect of oxone concentration on RhB degradation was studied and the results are presented in Fig. 10. It is worth mentioning that increasing oxone concentration from 0.02 to  $0.20 \text{ g L}^{-1}$  led to a faster and more efficient degradation of RhB from 54.4 to 99%. Meanwhile, the kinetic rate constant also increased from 0.0654 to  $0.1918 \text{ min}^{-1}$ . These results could be explained by the high concentration of free sulfate radicals formed at higher oxone concentration, which result in an increase in the rate of RhB degradation. Therefore, the optimal oxone concentration was about  $0.1 \text{ g L}^{-1}$  for the degradation of RhB on the  $\text{CoFe}_2\text{O}_4/\text{GO}$  catalyst.

The effect of reaction temperature on RhB degradation was also investigated by varying the reaction temperatures from 20 to 30 to  $40 \text{ }^\circ\text{C}$ ; the experimental findings are presented in Fig. 11. It can be observed that the degradation rate of RhB increases from  $0.135$  to  $1.085 \text{ min}^{-1}$  with increasing temperature from 20 to  $40 \text{ }^\circ\text{C}$ . These results could be explained by the high concentrations of free sulfate radicals generated at high temperature.

To further evaluate the effect of the  $\text{CoFe}_2\text{O}_4/\text{GO}$  nanocatalyst on the process kinetics, important parameters associated with the energetic aspects of the reaction, such as activation energy, ( $E_a$ ) play a crucial role. The activation energy ( $E_a$ ) of the degradation of RhB over the  $\text{CoFe}_2\text{O}_4/\text{GO}$  catalyst was evaluated by plotting  $\ln(k)$  versus  $1000/T$  according to the Arrhenius equation of  $\ln(k) = \ln(A) - E_a/RT$ , where  $k$  is the rate constant,  $R$  is the universal gas constant ( $8.314 \text{ J mol}^{-1} \text{ K}$ ) and  $A$  is the pre-exponential. The  $E_a$  value of  $79.24 \text{ kJ mol}^{-1}$  was obtained from the slope of the fitted equation by linear regression

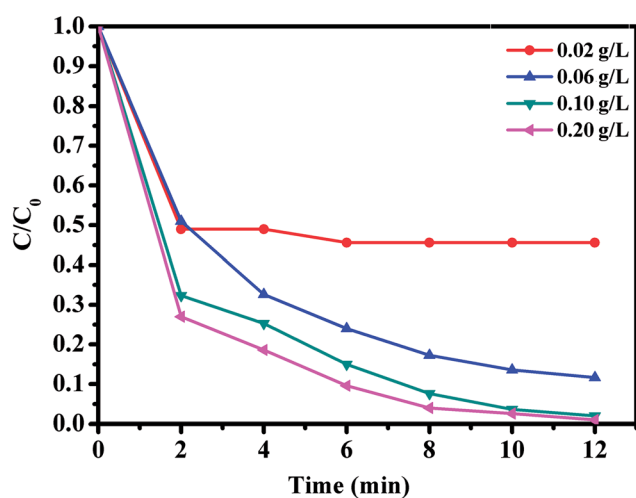


Fig. 10 Effect of oxone concentration on RhB degradation over  $\text{CoFe}_2\text{O}_4/\text{GO}$ . Reaction conditions:  $[\text{RhB}] = 0.03 \text{ mmol L}^{-1}$ , amount of catalyst =  $10 \text{ mg}$ ,  $T = 25 \text{ }^\circ\text{C}$ .

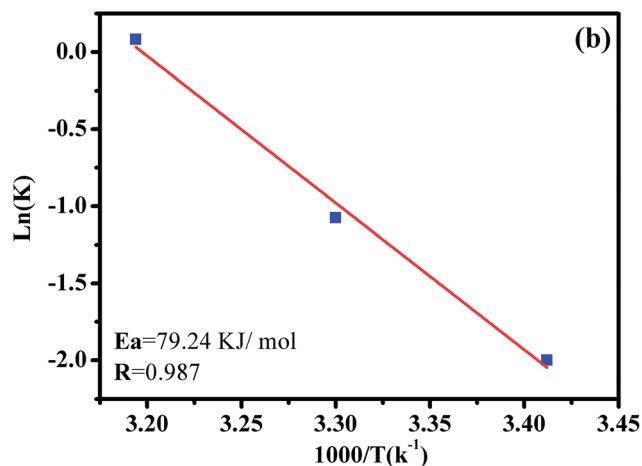
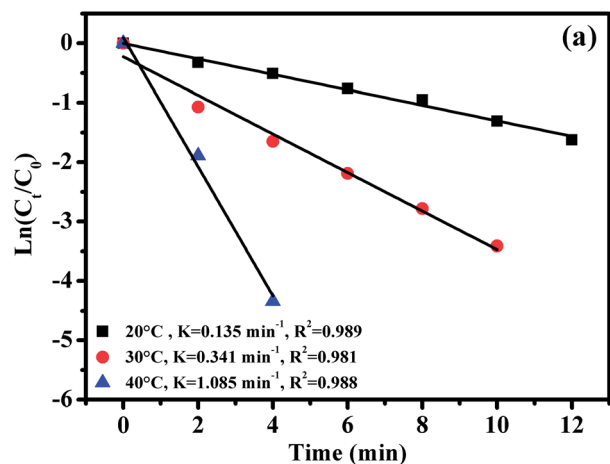


Fig. 11 The effect of reaction temperature on RhB degradation over the  $\text{CoFe}_2\text{O}_4/\text{GO}$  catalyst (a); the Arrhenius plot with linear regression (b); reaction conditions:  $[\text{RhB}] = 0.03 \text{ mmol L}^{-1}$ , amount of catalyst =  $10 \text{ mg}$  and  $0.1 \text{ g L}^{-1}$  of oxone at different temperatures.

( $R^2 = 0.987$ ). This  $E_a$  value is comparable to those of the highest active heterogeneous catalysts ever reported, e.g.,  $\text{Co}/\text{active carbon}$  ( $59.7 \text{ kJ mol}^{-1}$ ),<sup>11</sup>  $\text{Co}_3\text{O}_4/\text{SiO}_2$  ( $61.7\text{--}75.5 \text{ kJ mol}^{-1}$ )<sup>36</sup> and  $\text{Co}/\text{ZSM-5}$ , ( $69.7 \text{ kJ mol}^{-1}$ ),<sup>17</sup> which indicates that  $\text{CoFe}_2\text{O}_4/\text{GO}$  can be considered a promising heterogeneous catalyst for the PMS oxidation process.

The effect of RhB concentration was studied by varying the concentration of RhB and the experimental findings are presented in Fig. 12. Upon decreasing RhB concentration from  $0.01$  to  $0.03 \text{ mmol L}^{-1}$ , the degradation rate of RhB over  $\text{CoFe}_2\text{O}_4/\text{GO}$  increased significantly. Indeed, RhB was almost completely removed within 6 min at the RhB concentration of  $0.01 \text{ mmol L}^{-1}$ , while it was removed within 12 min at the concentration of  $0.03 \text{ mmol L}^{-1}$ .

The influence of initial pH values on RhB degradation over the  $\text{CoFe}_2\text{O}_4/\text{GO}$  catalyst was explored by adjusting the solution pH to 3.5, 6, 7, 8, 10 and 11. As shown in Fig. 13, the initial pH has a significant influence on the degradation efficiency of RhB. Based on the results obtained, we observed that the RhB degradation conducted at an initial pH of 3.5 and 7.0 was faster (decolorization efficiency of 98% at about 12 min) due to the





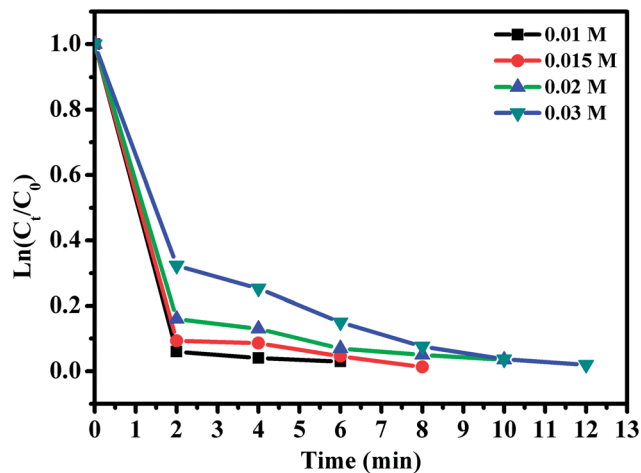


Fig. 12 Effect of RhB concentration. Reaction conditions: [PMS] = 0.1 mmol L<sup>-1</sup>; amount of catalyst = 10 mg, *T* = 25 °C.

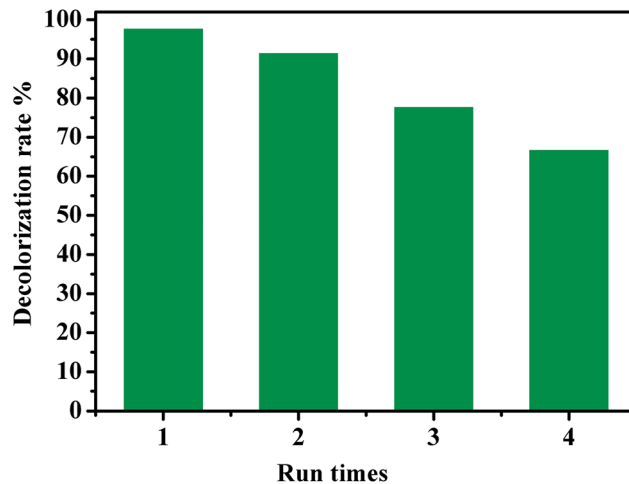


Fig. 14 Reuse performance of the CoFe<sub>2</sub>O<sub>4</sub>/GO catalyst in RhB degradation. Reaction conditions: [RhB] = 0.03 mmol L<sup>-1</sup>, [PMS] = 0.10 mmol L<sup>-1</sup>, amount of catalyst = 10 mg, *T* = 25 °C.

electrostatic attraction between the negative charge of the CoFe<sub>2</sub>O<sub>4</sub>/GO catalyst at low pH (Fig. 13c) and the positive charge of RhB. It is also noteworthy that there was no obvious impact on the RhB degradation when the initial pH value changed in the range of 3.5–7. Moreover, at high initial pH values of 10.0 and 11.0, the decolorization rates were 40% and 17%, respectively, which can be explained by the deprotonation of the carboxyl group of RhB and the transformation of the cationic form of RhB into zwitterionic form.

The recyclability of a catalyst is advantageous for its commercialization and industrialization. To explore the

reusability of our catalytic system, CoFe<sub>2</sub>O<sub>4</sub>/GO nanocomposite was employed as a recyclable catalyst in the degradation of RhB by PMS over four cycles. After each cycle, the catalyst was easily separated by an external magnet and washed successively by water and dichloromethane. As shown in Fig. 14, it was found that the catalytic performance of the recovered catalyst remained nearly the same for the second successive run. Although the catalytic activity slightly diminished, 67% of decolorization rate was still achieved in the fourth run, indicating that CoFe<sub>2</sub>O<sub>4</sub>/GO nanocatalysts exhibited good



Fig. 13 Effect of pH on RhB degradation over the CoFe<sub>2</sub>O<sub>4</sub>/GO catalyst (a, b); point zero charge of CoFe<sub>2</sub>O<sub>4</sub>/GO. Reaction conditions: [RhB] = 0.03 mmol L<sup>-1</sup>, [PMS] = 0.10 mmol L<sup>-1</sup>, amount of catalyst = 10 mg, *T* = 25 °C.



